

# Onset of Fermi Degeneracy in a Trapped Atomic Gas

B. DeMarco and D. S. Jin\*†

An evaporative cooling strategy that uses a two-component Fermi gas was employed to cool a magnetically trapped gas of  $7 \times 10^5$   $^{40}\text{K}$  atoms to 0.5 of the Fermi temperature  $T_F$ . In this temperature regime, where the state occupation at the lowest energies has increased from essentially zero at high temperatures to nearly 60 percent, quantum degeneracy was observed as a barrier to evaporative cooling and as a modification of the thermodynamics. Measurements of the momentum distribution and the total energy of the confined Fermi gas directly revealed the quantum statistics.

Fermions, such as electrons, protons, and neutrons, compose all of the matter around us, and phenomena derived from the quantum degeneracy of Fermions are ubiquitous in nature. Fermi-Dirac (FD) statistics governs the structure and behavior of such diverse systems as atoms, nuclei, electrons in metals, and white dwarf and neutron stars. However, Fermi systems are generally dense and strongly interacting. The only realization of a low-density Fermi system up to the present has been a dilute solution of liquid  $^3\text{He}$  dissolved in superfluid  $^4\text{He}$  (1). We report here the creation of a nearly ideal Fermi gas composed of atoms cooled to the regime where effects of quantum statistics can be observed.

This ultracold atomic gas constitutes a dilute system in which the interparticle interactions are weak and readily treated theoretically. Furthermore, fundamental control over the interactions is available, for example, through the recently realized magnetic field Feshbach resonances (2). In addition, the inhomogeneous trapping potential leads to a spatial separation of high- and low-energy atoms, giving rise to a Fermi surface that is manifest in position as well as in momentum. Features comparable with those listed above have already been demonstrated and exploited in studies of dilute-gas Bose-Einstein condensates (3). Hence, an ultracold atom gas of Fermions is an ideal system for quantitative study of quantum statistical effects in a controlled environment. Novel phenomena predicted for this system include shell structure (4), linewidth narrowing in spontaneous emission (5, 6), suppression of inelastic and elastic collisions (7, 8), changes in the excitation spectrum and damping rates (9, 10), and the emergence of a zero-sound mode at

low temperature (11). Another prospect in this system is the possibility of a phase transition at very low temperature to a superfluid state of Cooper-paired atoms (12).

We magnetically confined and evaporatively cooled a gas of Fermionic atoms,  $^{40}\text{K}$ , to temperatures  $T$  below 300 nK. The gas enters a regime where  $T$  is less than the Fermi temperature  $T_F$  and quantum statistical effects become significant. We monitored the evaporative cooling efficiency by measuring the scaled temperature  $T/T_F$  as a function of the number of atoms  $N$  and probed the thermodynamics of the Fermi gas with time-of-flight optical imaging. The quantum statistics are directly observable in the momentum distribution and in the total energy of the ultracold, trapped Fermionic atom gas.

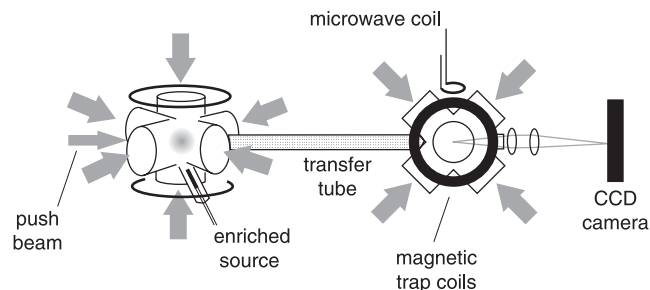
The  $^{40}\text{K}$  atoms are collected and pre-cooled optically in a double magneto-optic trap (MOT) apparatus (Fig. 1). In the first MOT, atoms are captured from a room-temperature vapor provided by a potassium atom source enriched in the Fermionic isotope  $^{40}\text{K}$  (13). A series of light pulses pushes the atoms to the second MOT located in a higher vacuum section of the apparatus (14) where the gas is Doppler-cooled to 150  $\mu\text{K}$  (15) before being loaded into a purely magnetic trap. A Ioffe-Pritchard-type magnetic trap (16) provides a cylindrically symmetric, harmonic potential with an axial frequency of  $\omega_z = 2\pi \times 19.5$  Hz and a variable radial frequen-

cy. The radial frequency, as well as the minimum magnetic field, can be smoothly varied from  $\omega_r = 2\pi \times 44$  Hz to  $2\pi \times 370$  Hz by changing the current in a pair of Helmholtz bias coils. The lifetime of atoms in the magnetic trap has an exponential time constant of 300 s limited by collisions with residual room-temperature atoms. This gives ample time for forced evaporation.

Forced evaporative cooling of Fermionic atoms to quantum degeneracy presents particular challenges because of the FD statistics. Evaporative cooling in the magnetic trap (17) relies on binary elastic collisions to rethermalize the gas after selective removal of the most energetic atoms. At the temperatures of interest (below 100  $\mu\text{K}$ ), these collisions are primarily s-wave in character and are prohibited between spin-polarized identical Fermions. Various schemes to circumvent this limit to evaporative cooling have been proposed, including sympathetic cooling between Fermionic and Bosonic species (18, 19) or enhancement of the p-wave collision rate by means of an applied dc electric field (20). Our strategy for cooling  $^{40}\text{K}$  involves magnetically trapping two spin states of the Fermionic species (21). In effect, we simultaneously cool two gases that maintain thermal equilibrium only through thermal contact with each other by means of allowed s-wave collisions. Runaway evaporation, in which the collision rate in the gas increases as the temperature decreases, thus requires a nearly equal mixture of the two spin states and balanced removal of energy from each component. These constraints necessitate selective removal of atoms from both spin state gases during evaporation.

For the experiment presented here we trapped a mixture of atoms in two magnetic sublevels,  $|F = 9/2, m_F = 9/2\rangle$  and  $|9/2, 7/2\rangle$ , of the hyperfine ground state having total atomic spin  $F = 9/2$  ( $m_F$  is the magnetic quantum number) (Fig. 2A). This particular mixture of spin states is metastable against  $m_F$  changing collisions at low  $T$  so that the number of atoms in each state is separately conserved. To selectively remove atoms in either spin state for evaporation we drive

**Fig. 1.** Schematic of the double-MOT apparatus used to trap and cool  $^{40}\text{K}$  atoms. The transfer tube permits differential pressure between the first MOT (left) and second MOT (right) and hexapole magnetic confinement for atoms in transit between the two glass cells. Atoms in the second MOT are transferred into a Ioffe-Pritchard-type magnetic trap where they are evaporatively cooled by a microwave field delivered by a small coil. After the atoms are released from the trap, the shadow that the atom cloud casts onto a resonant probe beam is imaged onto a charge-coupled device (CCD) array.



JILA, National Institute of Standards and Technology, and Physics Department, University of Colorado, Boulder, CO 80309-0440, USA.

\*Quantum Physics Division, National Institute of Standards and Technology, University of Colorado, Boulder, CO 80309-0440, USA.

†To whom correspondence should be addressed. E-mail: jin@jilau1.colorado.edu

REPORTS

microwave transitions with frequencies  $\nu_{9/2}$  and  $\nu_{7/2}$  ( $\sim 1.3$  GHz) to an untrapped spin state in the  $F = 7/2$  hyperfine level. Zeeman shifts, due to the interaction of the atomic magnetic moment  $\mu$  with the spatially varying magnetic field of the trap, cause these transitions to be nondegenerate and allow selective removal of the high-energy atoms present in either gas.

As illustrated in Fig. 2B, this type of evaporation can occur in three regimes set by the energy scales of the gas temperature compared with the trap's minimum magnetic field  $B_0$ . The kinetic energy scale  $k_B T$  sets the width of the cloud in the magnetic potential and hence the spread of microwave frequencies  $\delta\nu \sim k_B T/h$  that will remove atoms from the trap. Here  $k_B$  is Boltzmann's constant and  $h$  is Planck's constant. The trap bias field  $B_0$  sets the Zeeman shift  $\Delta\nu = \nu_{9/2} - \nu_{7/2}$  between the two microwave lines at the trap center. At relatively high  $T$  (case 1 in Fig. 2B) where  $\delta\nu \gg \Delta\nu$ , a single frequency removes atoms nearly equally from both spin states. At low  $T$  (case 3 in Fig. 2B) where  $\delta\nu \ll \Delta\nu$ , the microwave lines are distinct and two microwave frequencies are needed to cool both components of the gas in parallel. In the intermediate case (case 2, Fig. 2B) where  $\delta\nu \approx \Delta\nu$ , the application of any relevant microwave frequency will remove unequal numbers of atoms from each species. It is therefore impossible to efficiently cool through this regime with a microwave field.

To overcome this problem we controlled the evaporation regime through adiabatic changes in the magnetic trap strength, which affect both  $T$  and  $B_0$ . After  $\sim 10^8$  atoms are loaded into a relatively weak magnetic trap, an adiabatic ramp to a high- $\omega_r$  trap increases the collision rate for evaporation. The evap-

oration begins in this  $B_0 = 1.0$  gauss trap with a 60%/40% mixture of the  $m_F = 9/2$  and  $m_F = 7/2$  states at  $T \approx 1$  mK ( $T/T_F \approx 240$ ). In the first stage of evaporation, a single-frequency microwave field is applied to evaporatively cool the gas as in case 1 (Fig. 2B). When the condition  $\delta\nu \approx \Delta\nu$  is reached (at  $T/T_F \approx 1$ ), a second stage begins with an adiabatic ramp of the bias field to  $B_0 = 5.0$  gauss, resulting in a radial trap frequency  $\omega_r = 2\pi \times 137$  Hz. In this trap, evaporation uses a two-frequency microwave field (case 3, Fig. 2B) with a frequency difference that keeps the spin mixture constant to within 5%.

After evaporation an analysis of resonant absorption images, similar to that used to investigate Bose-Einstein condensates (22), was used to determine  $N$ ,  $T$ , and the momentum distribution of the Fermi gas. To simplify interpretation of these images, we produced a single-component gas of  $m_F = 9/2$  atoms by removing the  $m_F = 7/2$  atoms with a microwave sweep (23). To keep the remaining  $m_F = 9/2$  atoms in thermal equilibrium, we chose a time scale for the sweep that was slow compared with the collision rate in the sample. Indeed, this sweep provides the final evaporative cooling. The time-of-flight image was taken by suddenly switching off the current that provides the magnetic trapping field (always releasing from the  $B_0 = 5.0$  gauss trap) was switched off, which allowed the gas to expand freely for 15 to 20 ms. The absorption shadow, generated by illumination of the expanded gas with a 24- $\mu$ s pulse of light resonant with the  $4S_{1/2}$ ,  $F = 9/2$  to  $4P_{3/2}$ ,  $F = 11/2$  transition, was imaged onto a charge-coupled device array, and the optical depth was calculated. The probe beam, which travels along the double-MOT axis (Fig. 1), is circularly polarized and has a uniform inten-

sity profile with  $I/I_{\text{saturation}} = 0.05$ . The imaging system uses  $f/5$  optics and has a resolution better than 15  $\mu$ m, much smaller than the 270- $\mu$ m size of the smallest expanded atom cloud.

The quantum statistics dramatically influences the evaporative cooling of Fermions, as illustrated in a plot of the observed evaporation trajectory (Fig. 3). The trajectory is shown as  $T/T_F$  versus  $N$ , where  $T_F = \hbar/k_B (6\omega_r \omega_r^2 N)^{1/3}$  (Fig. 3) ( $\hbar = h/2\pi$ ) (24, 25). The value of  $T_F$ , which changes as  $N$  decreases during evaporation, is  $T_F = 0.6$   $\mu$ K for a million atoms in the  $\omega_r = 2\pi \times 137$  Hz trap. A measure of the efficiency of evaporation is the slope of this  $T/T_F$  versus  $N$  curve. Although  $T/T_F$  follows an efficient trend with  $N$  for the bulk of evaporation, the behavior changes drastically as  $T/T_F$  nears 0.5. For  $T/T_F \lesssim 0.5$ , the forced evaporation becomes grossly inefficient in reducing  $T/T_F$ , and many more atoms are removed to accomplish the same change in  $T$ .

This plunge in cooling efficiency does not coincide with any observed change in the atoms' loss or heating rate and is robust against changes in the details of evaporation. The behavior survives variation in the initial number of atoms and temperature of the sample, changes in the duration of the microwave sweep that removes  $m_F = 7/2$  atoms, changes in the evaporation timing, and even replacement of the second stage of evaporation with continued single-frequency removal of atoms in a lower  $B_0$  trap (as in case 1, Fig. 2B). In addition to the data presented in Fig. 3 obtained with the evaporation procedure described above, we observed that the reduction in evaporation efficiency always occurs near  $T/T_F \approx 0.5$ , even when we varied  $N$  and  $\omega_r$ . At the point where the evaporation effi-

**Fig. 2.** Hyperfine structure of the  $^{40}\text{K}$  ground states (A) and schematic representation of evaporation regimes (B). Trapping atoms in the  $m_F = 9/2$  and  $m_F = 7/2$  Zeeman sublevels of the  $F = 9/2$  ground state allows s-wave elastic collisions in the gas. The indicated microwave transitions  $\nu_{9/2}$  and  $\nu_{7/2}$  (shown with exaggerated Zeeman splittings) are driven for evaporation, selectively removing atoms from either spin component. Plotted in (B) is the fraction of atoms that would remain in each component versus the applied microwave frequency (arbitrary scale), with the frequency appropriate for evaporation  $\nu_{\text{evap}}$  indicated by a dotted line (note that lower microwave frequencies remove higher energy atoms). The calculation assumed a classical gas in which the microwave field removes all atoms above a particular energy. The high  $T$  (case 1), low  $T$  (case 3), and intermediate regimes (case 2) are distinguished by the spread of frequencies  $\delta\nu$  resonant with atoms in the trap compared with the Zeeman shift  $\Delta\nu$  at the trap center.

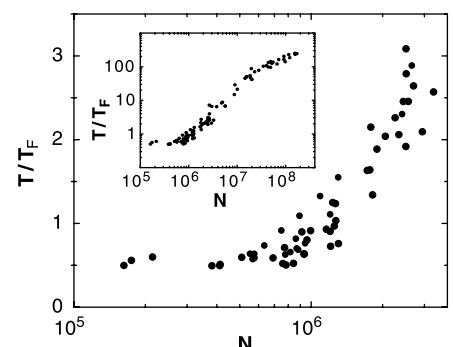
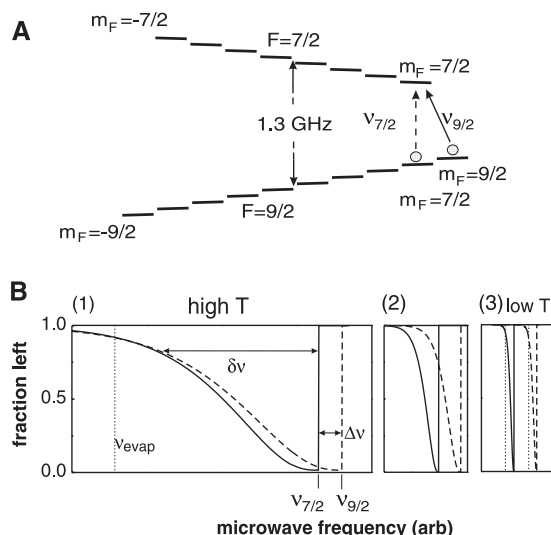


**Fig. 3.** Evaporation trajectory. A plot  $T/T_F$  versus  $N$  shows the result of evaporation; the inset displays the entire trajectory, starting at  $T/T_F \approx 240$  and  $N = 10^8$  atoms, and the main figure shows the low-temperature region. The bulk of the evaporation is very efficient, as seen in the large slope of the  $T/T_F$  versus  $N$  curve. However, the cooling process becomes limited at  $T/T_F \approx 0.5$ , where effects of FD statistics are observed in the momentum distribution of the gas.

ciency falls,  $N$  varied from  $3.5 \times 10^5$  to  $1.2 \times 10^6$  and  $\omega_r$  from 127 to 373 Hz, corresponding to a  $T_F$  of 0.36 to 1.0  $\mu\text{K}$ .

Although no quantitative theory exists yet, two general arguments (7) suggest that the onset of quantum behavior should lead to marked changes in the evaporation process. One effect of the quantum statistics is to alter the equilibrium size of the cloud in the magnetic trap by means of the Fermi pressure. This quantum mechanical pressure arises from the Pauli exclusion principle and causes a Fermi gas to resist compression, for example stabilizing white dwarf and neutron stars against gravitational collapse (26). In the magnetic trap, the confined gas approaches a fixed size as  $T$  approaches 0, with a root-mean-square radius of  $0.6R_F$  where  $R_F = \sqrt{2k_B T_F/m\omega^2}$  (24, 25); at  $T/T_F = 0.5$ , the radius of the gas is only  $0.9R_F$ . However, efficient “runaway” evaporation depends on the continual decrease in the size of the trapped cloud as  $T$  decreases and the accompanying increase in collision rate. Thus, the Fermi pressure will eventually negatively affect the evaporation.

A second effect of the quantum statistics on evaporation is Pauli blocking, which alters the dynamics of rethermalization after removal of high-energy atoms. At low  $T/T_F$  the atoms begin to form a Fermi sea arrangement, with the mean occupancy per state of the low-lying motional states approaching unity. At  $T/T_F = 0.5$ , for example, the occupancy of the lowest trap states is already 60%. The Pauli exclusion principle will begin to block the elastic collisions (8) essential to evaporation because

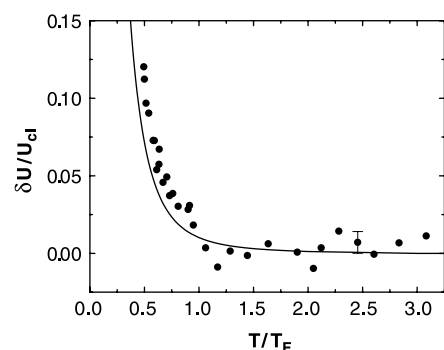


**Fig. 4.** Emergence of quantum degeneracy as seen in the energy of the trapped Fermi gas. A moment analysis was used to extract the energy of the gas from time-of-flight absorption images. The excess energy  $\delta U = U - U_{cl}$  is shown versus  $T/T_F$ , where  $U$  is the measured energy and  $U_{cl} = 3Nk_B T$  is the energy of a classical gas at the same temperature. Each point represents the average of two points from the evaporation trajectory shown in the main part of Fig. 3, and the single error bar shows the typical statistical uncertainty. The measured excess energy at low  $T/T_F$  agrees well with thermodynamic theory for a noninteracting Fermi gas (line).

the collisions will involve occupied low-energy final states. A quantitative understanding is lacking for how and when these effects become important in the forced evaporative cooling of Fermionic atoms.

In addition to witnessing a decrease in the evaporation efficiency, we observed the emerging quantum degeneracy in measurements of the total energy and the momentum distribution of the trapped Fermi gas. Classically, at high  $T$ , the gas has total energy  $U_{cl} = 3Nk_B T$  and a gaussian momentum distribution. At  $T = 0$ , however, the atoms occupy the energy levels of the harmonic confining potential in a Fermi sea arrangement with  $U_{FD} = \frac{3}{4} Nk_B T_F$ , and the Fermi pressure results in a parabolic momentum distribution (24). We measured the extra energy due to FD statistics and observed the transition between these two distributions by analyzing the optical depth images of expanded clouds.

A deviation from classical thermodynamics is exposed in a measurement of the total energy  $U$  of the trapped gas (Fig. 4). The total energy was obtained from the second moment calculated directly from absorption images of expanded clouds (27). This moment analysis of time-of-flight images is independent of any assumption of the exact statistical distribution. In addition, the effect of interactions on the expansion can be neglected because the mean field interaction energy is more than two orders of magnitude smaller than the trap potential energy for our single-component Fermi gas (10). In contrast to a dilute-gas Bose-Einstein condensate, where expansions typically exhibit a large effect due to interactions (28), the free expansion of the Fermi gas arises entirely from the kinetic energy of the sample.

The difference  $\delta U = U - U_{cl}$  between the measured energy and the classical energy at the same  $T$  is plotted in Fig. 4. The temperature  $T$  is determined from a fit to the periphery of the absorption image where the effects of the quantum statistics are reduced

because of the low mean occupancy at these high-momentum states (29). The emergence of excess energy in the gas due to FD statistics coincides with the change in evaporation efficiency and shows quantitative agreement with thermodynamic theory for a noninteracting Fermi gas (Fig. 4).

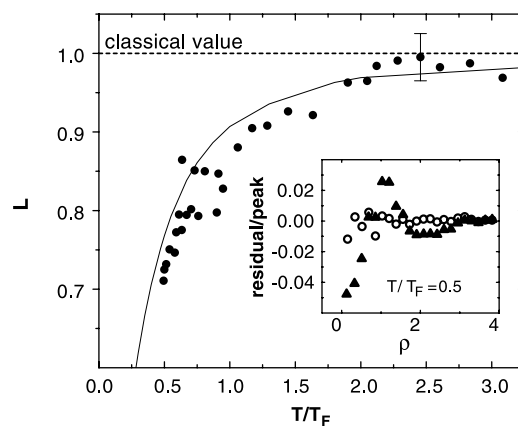
The excess energy due to FD statistics should be accompanied by a characteristic nongaussian momentum distribution. To explore the shape of the momentum distribution (6), we fit the cloud optical depth,  $OD(\rho)$ , to the following functional form that varies smoothly between the correct low- and high- $T$  limits:

$$OD(\rho) = \begin{cases} A \left(1 - \frac{\rho^2}{R^2}\right)^2 & , 1 - \frac{\rho^2}{R^2} \geq L \\ B e^{-\frac{\rho^2}{2}} & , \text{otherwise} \end{cases} \quad (1)$$

Here,  $\rho$  is a scaled distance  $\rho = \sqrt{x^2/\sigma_x^2 + z^2/\sigma_z^2}$  from the peak of the distribution, and  $A$ ,  $\sigma_x$ ,  $\sigma_z$ , and  $L$  are fit parameters. The requirement of continuity of the function and its first derivative at the boundary of the inner quartic and the outer gaussian form fixes the parameters  $B$  and  $R$ . The parameter  $L$  characterizes the deviation from the classical gaussian profile with  $L = 1$  at  $T/T_F \gg 1$  and  $L = 0$  at  $T/T_F = 0$ .

The data in Fig. 5 show the onset of a clear deviation from a gaussian momentum distribution ( $L = 1$ ) as  $T$  decreases below  $T_F$ . At low  $T/T_F$  the best fit value of the parameter  $L$  decreases from the classical value  $L = 1$  as the momentum distribution becomes nongaussian. This nongaussian character of the time-of-flight images can also be seen in an analysis of fit residuals that uses azimuthally averaged data. When low  $T/T_F$  images are fit to the classical gaussian distribution, a pattern appears in the fit residuals as a function of scaled radius  $\rho$  (Fig. 5, inset). At these low temperatures, fits to the function in Eq. 1 typically give a factor of 3 improvement in the reduced  $\chi^2$  compared with the simple gaussian fit. The deformation of the momen-

**Fig. 5.** Emergence of quantum degeneracy as seen in the shape of the momentum distribution. Surface fits to the same absorption images used for Fig. 4 reveal the nongaussian character of the momentum distribution at low  $T/T_F$ . For a particularly low noise image at  $T/T_F = 0.5$  the inset shows fit residuals normalized by the peak  $OD$  versus the scaled cloud radius  $\rho$ . A classical gaussian fit (solid triangles) is contrasted with the nongaussian fitting function from Eq. 1 (open circles). The main figure shows the fit parameter  $L$  of the nongaussian form versus  $T/T_F$ . For a classical gas  $L = 1$ ; for a Fermi gas at  $T/T_F = 0$ ,  $L = 0$ . The data compare well to theory (line), in which interactions are neglected and the distribution is calculated with the Thomas-Fermi approximation (24).



tum distribution observed in the nongaussian fits signals the onset of FD quantum degeneracy, as evidenced by the good agreement between the data and the theory line presented in Fig. 5. In fact, the comparison with theory suggests that our lowest temperatures are actually closer to  $T/T_F = 0.4$ , consistent with our 20% systematic uncertainty in  $T/T_F$  (primarily due to uncertainty in  $N$ ) (30).

We detected the emergence of quantum degeneracy in a trapped gas of Fermionic atoms and observed a barrier to the evaporative cooling process in a two-component Fermi gas below  $0.5 T_F$ . We observed a nonclassical momentum distribution and found that the total energy of the gas is larger than the classical expectation. This excess energy is a manifestation of the Pauli exclusion principle that gives rise to an expanded momentum distribution at low  $T/T_F$  by forcing the atoms to fill higher motional states of the harmonic trapping potential. Even as  $T$  approaches zero, an ideal Fermi gas still has  $\frac{3}{4} k_B T_F$  energy per particle; indeed, at our lowest  $T/T_F \approx 0.5$  we measured an energy that is only 2.2 times this  $T = 0$  limit. Reaching this quantum regime in the dilute Fermi gas extends the field of quantum degenerate gases and sets the stage for further experimental probes of a Fermi sea of atoms.

References and Notes

1. See, for example, E. P. Bashkin and A. E. Meyerovich, *J. Phys. Colloq. France* **41**, C7-61 (1980).
2. S. Inouye et al., *Nature* **392**, 151 (1998); Ph. Courteille, R. S. Freeland, D. J. Heinzen, F. A. van Abeelen, B. J. Verhaar, *Phys. Rev. Lett.* **81**, 69 (1998); J. L. Roberts et al., *ibid.*, p. 5109; V. Vuletic, A. J. Kerman, C. Chin, S. Chu, *ibid.* **82**, 1406 (1999).
3. For recent reviews, see E. A. Cornell, J. R. Ensher, C. E. Wieman, online abstract available at <http://xxx.lanl.gov/abs/cond-mat/9903109>; W. Ketterle, D. S. Durfee, D. M. Stamper-Kurn, online abstract available at <http://xxx.lanl.gov/abs/cond-mat/9904034>
4. J. Schneider and H. Wallis, *Phys. Rev. A* **57**, 1253 (1998); G. M. Bruun and K. Burnett, *ibid.* **58**, 2427 (1998).
5. K. Helmerson, M. Xiao, D. Pritchard, International Quantum Electronics Conference 1990, book of abstracts (IEEE, New York, 1990), abstr. QTHH4; Th. Busch, J. R. Anglin, J. I. Cirac, P. Zoller, *Europhys. Lett.* **44**, 1 (1998); J. Ruostekoski and J. Javanainen, *Phys. Rev. Lett.* **82**, 4741 (1999).
6. B. DeMarco and D. S. Jin, *Phys. Rev. A* **58**, R4267 (1998).
7. J. M. K. V. A. Koelman, H. T. C. Stoof, B. J. Verhaar, J. T. M. Walraven, *Phys. Rev. Lett.* **59**, 676 (1987).
8. G. Ferrari, *Phys. Rev. A* **59**, R4125 (1999).
9. G. Bruun and C. Clark, online abstract available at <http://xxx.lanl.gov/abs/cond-mat/9905263>
10. L. Vichi and S. Stringari, online abstract available at <http://xxx.lanl.gov/abs/cond-mat/9905154>
11. S. K. Yip and T. L. Ho, *Phys. Rev. A* **59**, 4653 (1999).
12. H. T. C. Stoof, M. Houbiers, C. A. Sackett, R. G. Hulet, *Phys. Rev. Lett.* **76**, 10 (1996); M. A. Baranov and D. S. Petrov, *Phys. Rev. A* **58**, R801 (1998); M. Houbiers and H. T. C. Stoof, *ibid.* **59**, 1556 (1999); G. Bruun, Y. Castin, R. Dum, K. Burnett, online abstract available at <http://xxx.lanl.gov/abs/cond-mat/9810013>.
13. B. DeMarco, H. Rohner, D. S. Jin, *Rev. Sci. Instrum.* **70**, 1967 (1999).
14. C. J. Myatt, N. R. Newbury, R. W. Ghrist, S. Loutzenhiser, C. E. Wieman, *Opt. Lett.* **21**, 290 (1996).
15. In our experiment we saw no evidence for sub-Doppler cooling processes that are used to bring

- some alkali gases to much colder temperatures. However, sub-Doppler cooling of  $^{40}\text{K}$  is reported in G. Modugno, C. Benko, P. Hannaford, G. Roati, M. Inguscio, online abstract available at <http://xxx.lanl.gov/abs/cond-mat/9908102>
16. V. V. Gott, M. S. Ioffe, V. G. Tel'kovskii, *Nucl. Fusion* (1962 suppl.), 1045 (1962); *ibid.*, p. 1284; D. E. Pritchard, *Phys. Rev. Lett.* **51**, 1336 (1983).
17. H. F. Hess, *Phys. Rev. B* **34**, 3476 (1986); H. F. Hess et al., *Phys. Rev. Lett.* **59**, 672 (1987).
18. C. J. Myatt, E. A. Burt, R. W. Ghrist, E. A. Cornell, C. E. Wieman, *Phys. Rev. Lett.* **78**, 586 (1997).
19. W. Geist, L. You, T. A. B. Kennedy, *Phys. Rev. A* **59**, 1500 (1999); E. Timmermans and R. Côté, *Phys. Rev. Lett.* **80**, 3419 (1998).
20. W. Geist, A. Idrizbegovic, M. Marinescu, T. A. B. Kennedy, L. You, online abstract available at <http://xxx.lanl.gov/abs/cond-mat/9907222>
21. B. DeMarco, J. L. Bohn, J. P. Burke Jr., M. Holland, D. S. Jin, *Phys. Rev. Lett.* **82**, 4208 (1999).
22. J. R. Ensher, D. S. Jin, M. R. Matthews, C. E. Wieman, E. A. Cornell, *ibid.* **77**, 4984 (1996).
23. The remaining gas was composed of 99%  $m_F = 9/2$  atoms, determined from a measurement of the cross-dimensional relaxation rate (21).
24. D. A. Butts and D. S. Rokhsar, *Phys. Rev. A* **55**, 4346 (1997).
25. I. F. Silvera and J. T. M. Walraven, *J. Appl. Phys.* **52**, 2304 (1981); J. Oliva, *Phys. Rev. B* **39**, 4204 (1989).
26. W. Greiner, L. Neise, H. Stöcker, *Thermodynamics and*

*Statistical Mechanics* (Springer-Verlag, New York, 1995), pp. 359–362.

27. The kinetic energy extracted from the time-of-flight absorption images equals half the total energy of the harmonically confined gas (from the equipartition theorem).
28. M. O.-Mewes et al., *Phys. Rev. Lett.* **77**, 416 (1996); M. J. Holland, D. S. Jin, M. L. Chiofalo, J. Cooper, *ibid.* **78**, 3801 (1997).
29.  $T$  is obtained from the widths of the outer gaussian,  $\sigma_x$  and  $\sigma_z$ , in fits of the form given in Eq. 1. Although the effects of the FD statistics are less severe on the outer edges of the momentum distribution, these fits become less accurate as  $T/T_F$  decreases. We made a correction to  $T$  that is at most 7% based on the measured  $T/T_F$  and the results of identical fits to calculated (semiclassical) momentum distributions for an ideal Fermi gas.
30. The number of atoms  $N$  is calibrated by a fluorescence measurement, which has an uncertainty of  $\pm 50\%$  because of intensity variations across the laser beams. The trap frequencies are determined to better than  $\pm 5\%$  from center-of-mass oscillations of the trapped gas.
31. Supported by the National Institute of Standards and Technology, the NSF, and the Office of Naval Research. We thank C. Wieman, E. Cornell, and the other members of the JILA BEC group for useful discussions.

19 July 1999; accepted 16 August 1999

## A Capacitance Standard Based on Counting Electrons

Mark W. Keller,<sup>1\*</sup> Ali L. Eichenberger,<sup>1</sup> John M. Martinis,<sup>1</sup> Neil M. Zimmerman<sup>2</sup>

A capacitance standard based directly on the definition of capacitance was built. Single-electron tunneling devices were used to place  $N$  electrons of charge  $e$  onto a cryogenic capacitor  $C$ , and the resulting voltage change  $\Delta V$  was measured. Repeated measurements of  $C = Ne/\Delta V$  with this method have a relative standard deviation of  $0.3 \times 10^{-6}$ . This standard offers a natural basis for capacitance analogous to the Josephson effect for voltage and the quantum Hall effect for resistance.

In the past four decades, there has been an accelerating trend in metrology toward standards based on fundamental quantum properties of nature. Until 1960, all units in what is now the International System of Units (SI) were based on carefully constructed artifacts and classical physics ( $I$ ). Quantum physics first entered the SI in 1960, when the definition of the meter was based on the wavelength of radiation from a transition in the Kr atom. A voltage standard based on the Josephson effect was first adopted in 1972 and refined in 1990, and a resistance standard based on the quantum Hall effect was adopted in 1990 (2, 3). For capacitance, the best existing standards are known as “calculable capacitors” and rely on a special arrangement of several electrodes such that the capaci-

tance per unit length is related to the permittivity of free space (a defined constant in the SI) (4). Realizing such a standard requires precise alignment of electrodes of order 1 m in length, one of which must be movable, and compensation of end effects in order to make a system of finite length behave like an infinite system over a limited range. With the development over the past decade of single-electron tunneling (SET) devices that can precisely manipulate and detect single electrons (5), it is now possible to create a capacitance standard based on the quantization of electric charge (6). Such a standard, which we describe here, places capacitance metrology on a quantum basis and is a natural complement to the voltage and resistance standards adopted in 1990 (7).

Our capacitance standard combines SET devices and a low-loss cryogenic capacitor. We explain the operation of the standard, demonstrate its repeatability and uncertainty, and consider the prospects for developing our prototype into a practical calibration system. This stan-

<sup>1</sup>National Institute of Standards and Technology, Boulder, CO 80303, USA. <sup>2</sup>National Institute of Standards and Technology, Gaithersburg, MD 20899, USA.

\*To whom correspondence should be addressed. E-mail: mark.keller@boulder.nist.gov